COMPUTER METHODS IN APPLIED MECHANICS AND ENGINEERING 53 (1985) 149–161
NORTH-HOLLAND

APPLICATION OF THE CVBEM TO NON-UNIFORM ST. VENANT TORSION

T.V. HROMADKA II and G.C. PARDOEN
Civil Engineering, University of California, Irvine, CA 92717, U.S.A.

Received 21 March 1984
Revised manuscript received 16 April 1985

The complex-variable boundary-element method, or CVBEM, is used to approximate the stress distribution associated with non-uniform St. Venant torsion problems. By specifying either the normal- or tangential-force equilibrium equation in terms of the warping function or its conjugate, a Laplace equation results which is immediately tractable by using the CVBEM. A comparison of modeling results to known solutions indicates that the modeling technique is a useful approach for the estimation of interior stresses as well as for the evaluation of modeling error by means of an approximate boundary determined by the CVBEM approximation function.

0. Notation

- a, b characteristic dimension of cross-section,
- c nondimensional coefficient $0 < c < 0.5$,
- G shear modulus,
- G_k global trial function of degree k,
- H_j complex logarithm function for element j,
- P_j^k polynomial interpolation function of degree k for element j,
- R^{k-1} complex polynomial of degree $k-1$,
- s_j local coordinate for element j,
- w warping displacement,
- x x-coordinate of point on cross-section from center of twist,
- y y-coordinate of point on cross-section from center of twist,
- z nodal point on complex plane,
- $\hat{w}$ approximate solution of Laplace equation,
- Ω solution domain,
- δ_j weighting function for polynomial interpolation function for element j,
- $\hat{\psi}$ approximate warping function,
- $\psi(x, y)$ warping function,
- γ_j complex constant for element j,
- Γ simple closed contour on complex plane,
- Γ_j straight line segment for element j,
- $\hat{\Gamma}$ approximate boundary,
- $\hat{\phi}$ approximate conjugate function,
- $\phi(x, y)$ conjugate function,
- θ angle of twist/unit length,
- τ_{xz}, τ_{yz} shear stress,
- ξ, ζ dummy integration variable.

1. Introduction

The complex-variable boundary-element method (CVBEM) is a new approach for mathematically modeling two-dimensional potential problems [1]. Based on complex-variable

theory, an approximation function is developed by using a contour integration function based on the Cauchy integral equation. The resulting approximation function is analytic over the problem domain (i.e. possesses derivatives of all orders) and, therefore, both the real and imaginary parts exactly solve the Laplace equation over the problem domain.

Unlike other boundary integral methods, the CVBEM can be evaluated as to the error of approximation. Numerical methods develop primarily two sources of error; namely, errors in solving the governing partial differential equation and errors in satisfying the boundary conditions continuously. Domain methods such as finite elements or finite differences generally generate both types of errors in modeling potential problems, and the evaluation as to the modeling accuracy is typically estimated by comparing the change in estimated results by increasing the number of nodal points. Real-variable boundary-element methods typically satisfy the governing equation describing a potential (i.e., Laplace equation), but do not satisfy the boundary conditions continuously. Again, the error is estimated by increasing the number of nodes and comparing computed results. The CVBEM, on the other hand, provides for a unique error-evaluation technique which is easy to use. Because the CVBEM approximations *exactly satisfy the Laplace equation, there is no error in solving the governing equation.* However like the other numerical methods, the CVBEM approximation does not satisfy the boundary conditions continuously. But unlike the other numerical methods, the CVBEM can develop an exact representation of the modeling error by the determination of an 'approximate boundary' where the CVBEM approximation exactly satisfies the boundary conditions. That is, the approximate boundary is the locus of points where the CVBEM approximation meets the boundary condition values.

Using the approximate boundary, the analyst easily evaluates the accuracy of the CVBEM model. Should the CVBEM approximate boundary coincide with the actual problem boundary, then the exact solution to the boundary-value problem has been achieved. Generally, however, the usual procedure is for the analyst to determine the approximate boundary for a given nodal point placement scheme on the problem boundary. In regions where the approximate boundary differs significantly from the true boundary, more nodes are added and another approximate boundary developed. In this fashion, the analyst develops a highly accurate approximation analogous to an adaptive integration technique.

The approximative boundary error analysis technique provides a powerful modeling capability which sets the CVBEM apart from the other boundary and domain numerical methods. Usually the analyst develops an adequate CVBEM approximation within 5 or 6 attempts. Because the constructed version of the prototype is generally accepted to within a certain construction tolerance, the CVBEM analysis is typically terminated when the approximate boundary meets the construction tolerance criteria. Thus, the CVBEM model provides the exact solution for a probable construction of the prototype.

2. Numerical modeling approach

The complex-variable boundary-element method, or CVBEM [2], can be used to develop an approximation function $\omega(z)$ which is analytic in the domain of definition, Ω. Consequently, $\hat{\omega}(z)$ can be expressed as $\hat{\omega}(z) = \hat{\phi}(z) + i\hat{\psi}(z)$ where $\hat{\phi}(z)$ and $\hat{\psi}(z)$ are two-dimensional harmonic conjugate functions which satisfy the Laplace equation exactly in Ω.

The approximation function $\hat{\omega}(z)$ is developed by collocating the Cauchy integral equation at nodal points defined on the simple closed boundary, Γ. For m nodal points, m linear equations are generated which can be solved by the usual matrix solution techniques, such as Gaussian elimination. The resulting CVBEM approximation can then be used to calculate values of the potential function and other quantities of interest such as stresses in the interior of Ω.

3. CVBEM development

3.1. Discretization

Let Γ be a simple closed contour composed of straight line segments. Let Ω be the simply connected domain enclosed by Γ, where Γ is subdivided into m complex-variable boundary elements (CVBE) by

$$\Gamma = \bigcup_{j=1}^{m} \Gamma_j . \tag{1}$$

Define $(k+1)$ equidistant nodal points in each Γ_j such that $z_{j,1}$ and $z_{j,k+1}$ are the endpoints of Γ_j (Fig. 1 shows the global and local nodal numbering conventions). The global nodal coordinates are related to local nodal coordinates by $z_{j,1} = z_j$ and $z_{j,k+1} = z_{j+1,1} = z_{j+1}$. If one defines complex numbers $\bar{\omega}_{ji}$ at each node z_{ji}, then degree-k complex polynomials $P_j^k(z)$ are uniquely defined on each boundary element Γ_j.

3.2. Approximating functions

A global trial function of order k is defined by

$$G_k(z) = \sum_{j=1}^{m} \delta_j P_j^k(z), \quad z \in \Gamma, \tag{2}$$

where

$$\delta_j = \begin{cases} 1, & z \in \Gamma_j, \\ 0, & \text{otherwise}; \end{cases}$$

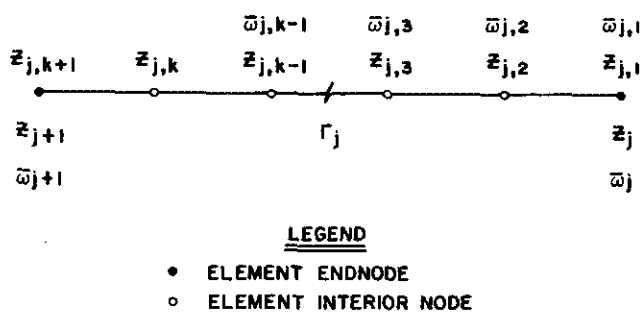

Fig. 1. $(k+1)$-node boundary-element Γ_j nodal definitions. ● element endnode; ○ element interior node.

$G_k(z)$ is continuous on Γ and

$$\lim_{\max|\Gamma_j|\to 0} G_k(z) = \omega(z), \tag{3}$$

where it is assumed that $\omega(z)$ is analytic on $\Omega \cup \Gamma$ and that each $\tilde{\omega}_{ji} = \omega(z_{ji})$.

Consider the approximation function $\hat{\omega}_k(z)$ defined by

$$\hat{\omega}_k(z) = \frac{1}{2\pi i} \int_{\Gamma} \frac{G_k(\zeta)\,d\zeta}{\zeta - z}, \quad z \notin \Gamma, \quad z \in \Omega. \tag{4}$$

From equation (2),

$$\int_{\Gamma} \frac{G_k(\zeta)\,d\zeta}{\zeta - z} = \int_{\zeta} \frac{\sum \delta_j P_j^k(\zeta)\,d\zeta}{\zeta - z} = \sum \int_{\Gamma_j} \frac{P_j^k(\zeta)\,d\zeta}{\zeta - z}. \tag{5}$$

On each Γ_j, define a local coordinate system by

$$\zeta_j = \zeta_j(s_j) = z_j(z_{j+1} - z_j)s_j, \quad \zeta_j \in \Gamma_j, \; 0 \leq s_j \leq 1. \tag{6}$$

It follows that

$$\int_{\Gamma_j} \frac{P_j^k(\zeta)\,d\zeta}{\zeta - z} = \int_0^1 \frac{P_j^k(s_j)\,ds_j}{s_j - \gamma_j}, \tag{7}$$

where $P_j^k(s_j) = P_j^k(\zeta_j(s_j))$, and $\gamma_j = (z - z_j)/(z_{j+1} - z_j)$ for $z \in \Gamma$.

Equation (7) is solved by factoring $(s_j - \gamma_j)$ from $P_j^k(s_j)$. Let $P_j^k(s_j)$ be of the form

$$P_j^k(s_j) = \sum_{i=0}^{k} a_{ji} s_j^i, \quad 0 \leq s_j^i \leq 1,$$

where the a_{ji} are complex constants. Division of $P_j^k(s_j)$ by $(s_j - \gamma_j)$ gives

$$\int_0^1 \frac{P_j^k(s_j)\,ds_j}{s_j - \gamma_j} = R_j^{k-1}(z) + P_j^k(\gamma_j)H_j, \tag{8}$$

where $R_j^{k-1}(z)$ is a complex polynomial of degree $k - 1$, and

$$H_j = \operatorname{Ln} \frac{z_{j+1} - z}{z_j - z} = \operatorname{Ln} \frac{d_{j+1}(z)}{d_j(z)} + i\theta_{j+1,j}(z). \tag{9}$$

Note that $d_j(z) = |z - z_j|$ and $\theta_{j+1,j}(z)$ is the central angle between points z_j, z_{j+1}, and z. Fig. 2 shows the special case as z approaches Γ in the limit.

From equations (4), (5), (7) and (8), summation of the CVBE contributions from the m boundary elements gives

$$2\pi i\hat{\omega}_k(z) = \sum R_j^{k-1}(z) + \sum P_j^k(\gamma_j)H_j \tag{10}$$

with $R^{k-1}(z) = \sum R_j^{k-1}(z)$, equation (10) simplifies to

$$\hat{\omega}_k(z) = \frac{1}{2\pi i}\left[R^{k-1}(z) + \sum P_j^k(\gamma_j)H_j\right]. \tag{11}$$

In (11), it is noted that the $P_j^k(\gamma_j)$ have the form of the assumed shape functions on each γ_j.

Letting node z_1 be on the branch cut of the complex logarithm function $\mathrm{Ln}(z - \zeta)$ such that $z \in \Omega$ and $\zeta \in \Gamma$ (see Fig. 3), then (11) can be expanded as

$$\hat{\omega}_k(z) = \frac{1}{2\pi i}R^{k-1}(z) - \frac{1}{2\pi i}\sum \Delta_j^{k-1}(z - z_j)\,\mathrm{Ln}\,(z - z_j) + P_m^k(z), \tag{12}$$

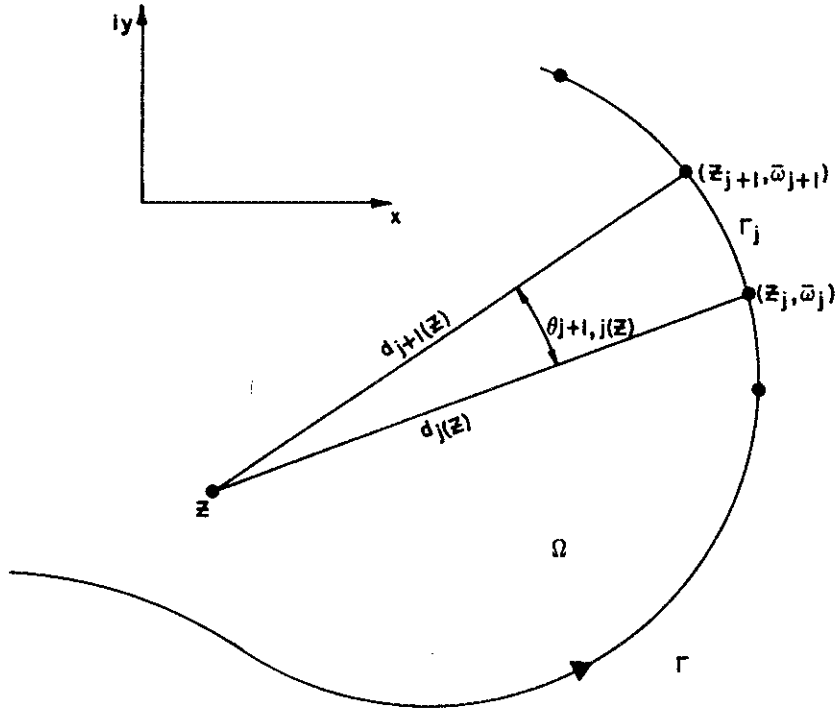

Fig. 2. CVBEM linear trial function geometry.

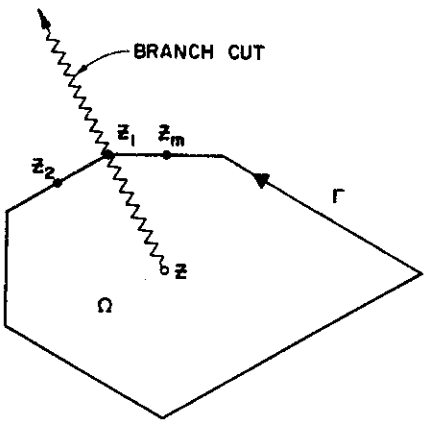

Fig. 3. Branch cut of the function $\mathrm{Ln}(z-\zeta)$, $\zeta \in \Gamma$.

where Δ_j^{k-1} is a polynomial of degree $(k-1)$ defined by

$$\Delta_j^{k-1} = \frac{(P_j^k(\gamma_j) - P_{j-1}^k(\gamma_{j-1}))}{(z - z_j)}, \tag{13}$$

and $\mathrm{Ln}(z - z_j)$ is the principal value of the logarithm function. From the continuity of $G_k(\zeta)$, it is seen that at the nodal coordinate z_j,

$$P_j^k(\gamma_j) - P_{j-1}^k(\gamma_{j-1}) = 0 \tag{14}$$

and that $(z - z_j)$ is a factor as shown in (13). In (12), the $P_m^k(z)$-term appears due to the circuit around the branch point of the multiple-valued function $\mathrm{Ln}(z-\zeta)$.

Letting

$$R^k(z) = \frac{1}{2\pi \mathrm{i}} R^{k-1}(z) + P_m^k(z),$$

then

$$\hat{\omega}_k(z) = R^k(z) - \frac{1}{2\pi \mathrm{i}} \sum_{j=1}^{m} \Delta_j^{k-1}(z - z_j) \mathrm{Ln}\,(z - z_j). \tag{15}$$

From (15), it is seen that $\hat{\omega}_k(z)$ is continuous over Ω and has removable singularities at each boundary-element endpoint (nodal coordinate z_j, $j = 1, 2, \ldots, m$). That is, $R^k(z)$ and Δ_j^{k-1} are continuous complex polynomials, and

$$\lim_{z \to z_j} (z - z_j) \mathrm{Ln}\,(z - z_j) = 0, \quad \text{i.e.} \quad \hat{\omega}_k(z_j) = R^k(z_j).$$

Note that since $\hat{\omega}_k(z)$ is analytic in Ω then $\hat{\omega}_k(z) = \hat{\phi}(z) + \mathrm{i}\hat{\psi}(z)$ where $\hat{\phi}(z)$ and $\hat{\psi}(z)$ are two-dimensional potential and stream functions which satisfy the Laplace equation exactly

over Ω. By forcing the approximation values of $\hat{\omega}_k(z)$ to be arbitrarily close (within some ε) to the boundary-condition values of $\omega(z)$ on Γ, then it is guaranteed by the maximum modulus theorem that the approximation of $\omega(z)$ is bounded by $|\omega(z)-\hat{\omega}(z)| \leq \varepsilon$, for all $z \in \Omega$.

Because the CVBEM results in a two-dimensional function which is an exact solution to the governing partial differential equation on Ω, convergence of $\hat{\omega}_k(z)$ to $\omega(z)$ is then achieved on $\Omega \cup \Gamma$ by forcing convergence on Γ. This is shown from (3) and (4) by

$$\lim_{\max|\Gamma_j|\to 0} \int_{\Gamma} \frac{G_k(\zeta)\,d\zeta}{\zeta - z} = \int_{\Gamma} \frac{\lim_{\max|\Gamma_j|\to 0} G_k(\zeta)\,d\zeta}{\zeta - z} = \int_{\Gamma} \frac{\omega(\zeta)\,d\zeta}{\zeta - z} = 2\pi i \omega(z)\,. \tag{16}$$

4. Modeling strategy

The numerical modeling strategy is to first use the CVBEM by collocating (15) at each nodal point specified on Γ (in the limit as z approaches Γ from inside Ω). Generally, only one nodal value of either ϕ or ψ is known at each nodal point. Consequently for m nodes specified on Γ, there are $2m$ values of $\{\phi_j, \psi_j\}$, and only m nodal values are known as boundary conditions. Collocating (4) at each node generates m equations for the m unknown nodal values. The resulting $m \times m$ matrix system results in the determination of the $\hat{\omega}_k(z)$ approximator which is analytic in Ω. That is, $\hat{\omega}_k(z)$ operates on the $2m$ nodal values $\{\theta_j, \psi_j\}$ and the coordinate z.

The second step is to develop an analytic continuation of the $\hat{\omega}_k(z)$ approximator by using equation (15), which matches the specified and computed $2m$ nodal values of Γ. The advantage of using (15) is that the Cauchy integral of (4) has the property that

$$\hat{\omega}_k(z) = \begin{cases} \hat{\omega}_k(z), & z \in \Omega \cup \Gamma, \\ 0, & z \notin \Omega \cup \Gamma. \end{cases} \tag{17}$$

The need for using equation (15) becomes apparent when determining the approximate boundary which is associated with the CVBEM approximator functions, $\hat{\omega}_k(z)$.

The third step is to develop an approximate boundary, $\hat{\Gamma}$, upon which $\hat{\omega}_k(z)$ satisfies the problem boundary conditions. For stress-free boundary conditions, $\hat{\Gamma}$ is the collection of points defined by

$$\hat{\Gamma} = \{z : \hat{\phi}(z) = \tfrac{1}{2}|z^2|\}\,, \tag{18}$$

where $\hat{\omega}(z) = \hat{\phi}(z) + i\hat{\psi}(z)$. Also $|z|^2 = x^2 + y^2$ where $|z|$ is measured from a selected central point in Ω. If $\hat{\Gamma}$ coincides with Γ, then necessarily $\hat{\omega}(z) = \omega(z)$ on $\Omega \cup \Gamma$. The utility of the approximate boundary concept is in the evaluation of the approximation error. Instead of the analysis of abstract error quantities, the goodness of approximation is determined by visually inspecting the closeness-of-fit between $\hat{\Gamma}$ and Γ. In those regions, where $\hat{\Gamma}$ deviates substantially from Γ, additional nodes are placed to reduce the approximation errors from using the selected shape functions.

5. Examples

As an example of the complex-variable boundary-element method consider the twisting behavior of a homogeneous, isotropic shaft of an arbitrary, but uniform, cross-section that is fixed at one end and subjected to a twisting couple at the other end. If the force and deformation behavior is of interest at some location somewhat removed from either end, then the stress and strain characteristics of the cross-section are described by either of the following equations [2]:

$$\frac{\partial^2\psi(x, y)}{\partial x^2}+\frac{\partial^2\psi(x, y)}{\partial y^2}=0\,, \tag{19}$$

$$\frac{\partial^2\phi(x, y)}{\partial y^2}+\frac{\partial^2\phi(x, y)}{\partial y^2}=0\,. \tag{20}$$

The quantity $\psi(x, y)$ is the warping function of the cross-section whereas $\phi(x, y)$ is the conjugate function of $\psi(x, y)$. If the warping function is known over the cross-section, then the out-of-plane warping displacement and the in-plane shear stresses can be calculated from the expressions

$$w=\theta\psi(x, y)\,,\qquad \tau_{xz}=G\theta\left\{\frac{\partial\psi(x, y)}{\partial x}-y\right\},\qquad \tau_{yz}=G\theta\left\{\frac{\partial\psi(x, y)}{\partial y}+x\right\}. \tag{21}$$

In the above expressions θ is the angle of twist/unit length, G is the shear modulus, and x, y denote the coordinates of a point located from the center of twist. Furthermore it should be noted that z represents a coordinate axis and should not be confused with the complex variable $z=x+iy$. If, on the other hand, the problem is posed in terms of the complementary function $\phi(x, y)$ then the shear stresses are determined from

$$\tau_{xz}=G\theta\left\{\frac{\partial\phi(x, y)}{\partial y}-y\right\},\qquad \tau_{yz}=G\theta\left\{-\frac{\partial\phi(x, y)}{\partial x}+x\right\}. \tag{22}$$

While the form of equations (19) and (20) are identical, a solution strategy emerges depending on the manner in which the boundary conditions are specified. If the boundary condition of zero normal stress around the perimeter is posed, then a Neumann boundary condition, i.e. specified normal derivative, best describes the problem. In such a case the nonuniform torsion problem is best posed in terms of the warping function $\psi(x, y)$. If, on the other hand, the problem is posed in terms of zero shear stress around the perimeter, then a Dirichlet boundary condition, i.e. specified functions, best describes the problem. In such a case the problem is best posed in terms of the complementary function $\phi(x, y)$. While either solution method is well adapted for solid shafts, it is generally more convenient to operate directly with the warping function $\psi(x, y)$ rather than its conjugate $\phi(x, y)$ for hollow cross-sections.

The purpose of the following two examples is to compare the complex-variable boundary-element method with established solutions [3] for shaft cross-sections of smooth and sharp

corner profiles. In each of the application problems, the aforementioned modeling strength is used to develop a $\hat{\omega}(z)$ approximator over each domain and an associated approximate boundary $\hat{\Gamma}$ is determined for comparison with the true boundary Γ by using the expression $\hat{\omega}(z)$ given in (15). In each application, nodal points were added at regions of high discrepancy between Γ and $\hat{\Gamma}$ after an initial modeling attempt. Using the modified nodal point placement, further attempts were made to develop a $\hat{\omega}(z)$ which better fit the specified boundary conditions. The resulting approximate boundaries are shown with the actual boundaries in the figures.

Consider first the torsion of a solid elliptical cross-section with major axis a and minor axis b. The shear-stress-free boundary condition can be expressed in terms of the conjugate function $\phi(x, y)$ expressed on the boundary as

$$\phi(x, y) = \tfrac{1}{2}(x^2 + y^2). \tag{23}$$

The conjugate function $\phi(x, y)$ as well as the shear stresses can be shown to be

$$\phi(x, y) = \tfrac{1}{2}(x^2 + y^2) - a^2b^2(x^2/a^2 + y^2/b^2 - 1)(a^2 + b^2), \tag{24}$$

$$\tau_{xz} = -G\theta(2ya^2)/(a^2 + b^2), \tag{25}$$

$$\tau_{yz} = G\theta(2xb^2)/(a^2 + b^2). \tag{26}$$

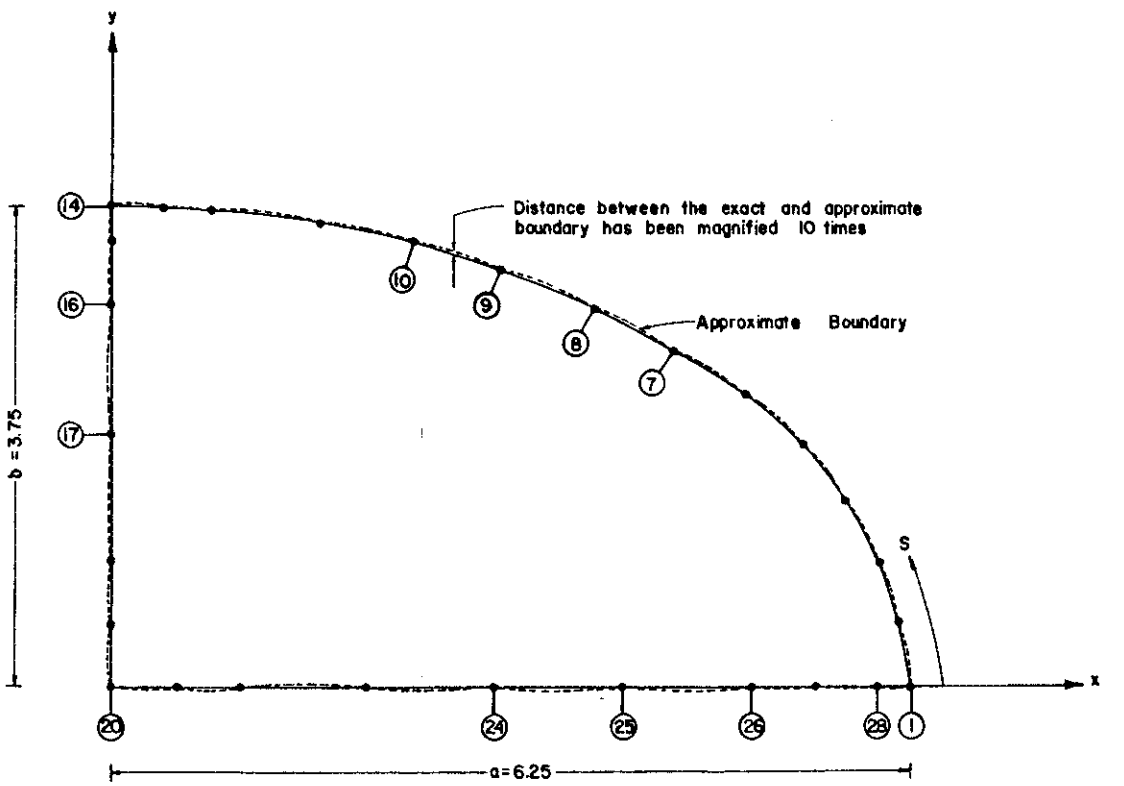

Fig. 4. Approximate boundary for the elliptical section.

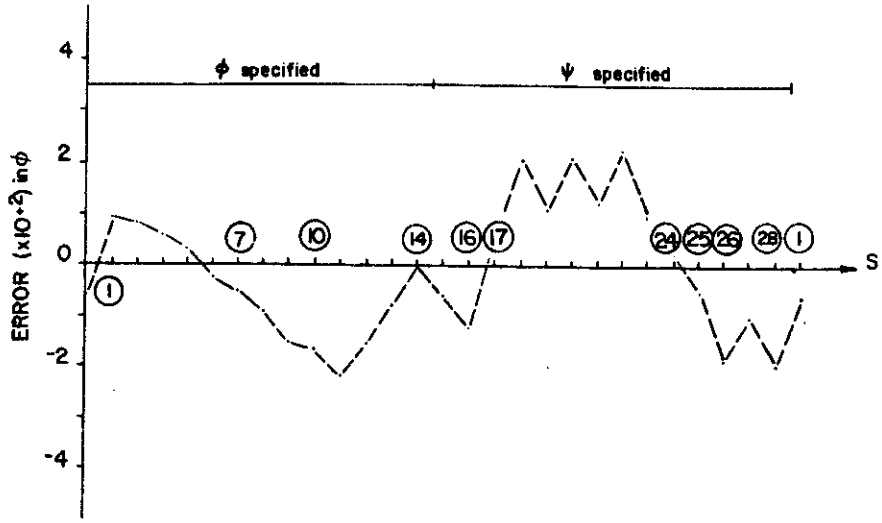

Fig. 5. CVBEM relative error for quarter elliptical section.

Fig. 4 displays the approximate boundary for the elliptical section whereas Fig. 5 shows the relative error

$$[(\phi_{\text{calculated}} - \phi_{\text{exact}})/\phi_{\text{exact}}]$$

for the 28-node model. A quarter model was chosen to take advantage of the problem symmetry as well as to demonstrate the imposition of ϕ boundary conditions along the exterior curved edge and ψ along the interior straight edge. Table 1 summarizes the exact and computed warping function and shear-stress values at points in Ω.

One of the distinct modeling advantages of the CVBEM is knowing where to define more boundary nodes. If one compares the computed boundary profile with that of the actual continuum being modeled, then it is a relatively routine task to add more nodes in the area of large approximate boundary discrepancy to obtain a closer approximation to the actual profile. Another advantage of CVBEM is the knowledge that the solution is exact for the boundary

Table 1
CVBEM vs. exact results; St. Vanant torsion—a quarter of the elliptical section model

x	y	ϕ	$\hat{\phi}$	$\Delta\phi$	τ_{xz}	$\hat{\tau}_{xz}$	$\Delta\tau_{xz}$	τ_{yz}	$\hat{\tau}_{yz}$	$\Delta\tau_{yz}$
1	1	10.3400	10.3767	0.35%	−1.4706	−1.5	2.00%	0.5294	0.5	5.55%
3	1	12.2224	12.2821	0.49%	−1.4706	−1.5	2.00%	1.5882	1.6	0.74%
5	1	15.9871	16.0281	0.44%	−1.4706	−1.5	2.00%	2.6470	2.7	2.00%
1	2	9.6341	9.6763	0.38%	−2.9421	−2.9	1.40%	0.5294	0.5	5.55%
3	2	11.5156	11.5588	0.37%	−2.9412	−3.0	1.40%	1.5882	1.6	0.74%
5	2	15.2812	15.2966	0.10%	−2.9412	−2.9	1.40%	2.6470	2.6	1.78%
1	3	8.4577	8.5070	0.58%	−4.4118	−4.4	0.27%	0.5294	0.5	5.55%
3	3	10.3400	10.3738	0.33%	−4.4118	−4.4	0.27%	1.5882	1.6	0.74%

that results from the solution technique. Obtaining more refined results is associated with simply obtaining a closer agreement of the approximate boundary with the true boundary. An additional programming advantage of the CVBEM is that although the model is one-dimensional (the boundary), it solves the two-dimensional Laplace equation with a relatively small amount of computer input. Further programming advantages such as small program size lend such a solution technique towards a microcomputer solution.

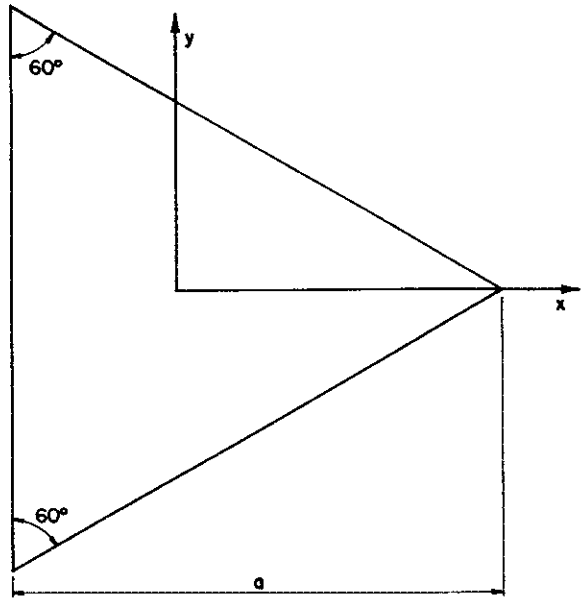

Fig. 6. Triangular section geometry.

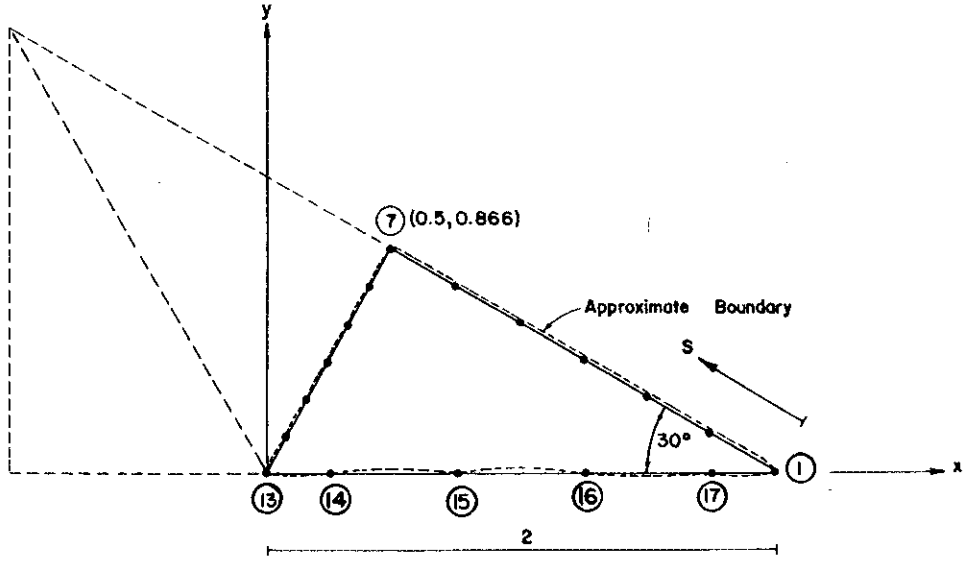

Fig. 7. CVBEM approximate boundary for 1/6 of the triangular section.

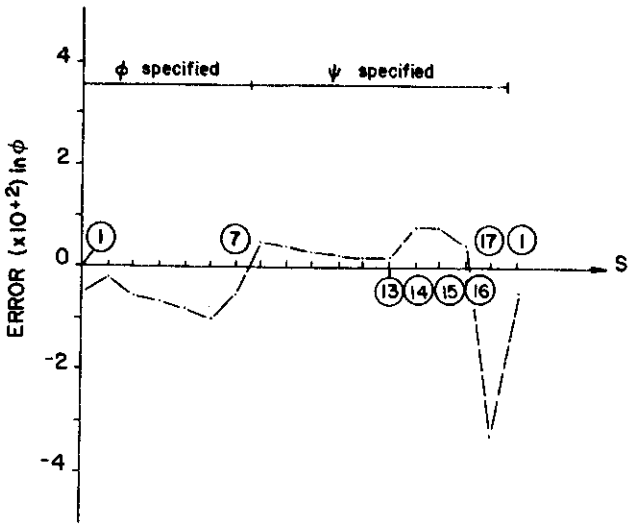

Fig. 8. CVBEM relative error for 1/6 of the triangular section.

As a second example, consider the sharp-edge equilateral triangular section shown in Fig. 6. The shear-stress-free boundary condition can be expressed in terms of the conjugate function $\phi(x, y)$ expressed on the boundary as

$$\phi(x, y) = \tfrac{1}{2}(x^2 + y^2)\,. \tag{27}$$

The conjugate function $\phi(x, y)$ as well as the shear stresses can be shown to be

$$\phi(x, y) = (x^3 - 3xy^2)/2a + \tfrac{2}{27}a^2\,, \tag{28}$$

$$\tau_{xz} = -G\theta\{y + 3xy/a\}\,, \tag{29}$$

$$\tau_{yz} = G\theta\{(3y^2 - 3x^2)/2a + x\}\,. \tag{30}$$

Fig. 7 displays the approximate boundary for the triangular section whereas Fig. 8 depicts the relative error $[(\phi_{\text{calculated}} - \phi_{\text{exact}})/\phi_{\text{exact}}]$ versus the perimeter coordinates for the 17-node model. Again, the relative error decreases as the number of nodal points are increased. Table 2 summarizes the exact and computed warping function and shear-stress values at various points.

Table 2
CVBEM vs. exact results; St. Venant torsion—a sixth of the trangular section model

x	y	ϕ	$\hat{\phi}$	$\Delta\phi$	τ_{xz}	$\hat{\tau}_{xz}$	$\Delta\tau_{xz}$	τ_{yz}	$\hat{\tau}_{yz}$	$\Delta\tau_{yz}$
0.5	0.25	0.6719	0.6820	1.50%	−0.375	−0.35	6.67%	0.40625	0.4	1.54%
0.5	0.50	0.6250	0.6355	1.68%	−0.750	−0.70	6.67%	0.50000	0.5	0.00%
0.5	0.75	0.5469	0.5560	1.66%	−1.125	−1.15	2.22%	0.65625	0.6	8.57%
1.0	0.25	0.8021	0.8150	1.61%	−0.500	−0.45	10.00%	0.53125	0.5	5.88%
1.0	0.50	0.7280	0.7196	1.15%	−1.000	−1.00	0.00%	0.62500	0.6	4.00%

6. Conclusion

The complex-variable boundary-element method has been demonstrated to be a viable analyses technique for nonuniform St. Venant torsion. Because the CVBEM approach results in an approximation function which exactly solves the Laplace equation, the only modeling error occurs in matching the prescribed boundary conditions continuously. However, the CVBEM offers a unique error analysis technique based on attempting to match an approximate boundary (where the CVBEM solution satisfies the boundary conditions) to the true problem boundary. When the approximate and true boundaries coincide, the CVBEM has developed the exact solution to the boundary-value problem.

References

[1] T.V. Hromadka II and G.L. Guymon, The complex variable boundary element method, Internat. J. Numer. Meths. Engrg. (1984).
[2] T.V. Hromadka II, The Complex Variable Boundary Element Method (Springer, Berlin, 1984).
[3] N.I. Muskhelishvili, Some Basic Problems of the Mathematical Theory of Elasticity (Noordhoff, Leyden, 1953).
[4] S.P. Timoshenko and J.N. Goodier, Theory of Elasticity (McGraw-Hill, New York, 3rd ed., 1970).